

Ultrafast All-Optical Switching Modulation of Terahertz Polarization Conversion Metasurfaces Based on Silicon

Qiangguo Zhou, Qinxi Qiu, Tuntan Wu, Yongzhen Li, and Zhiming Huang*

Cite This: *ACS Omega* 2023, 8, 48465–48479

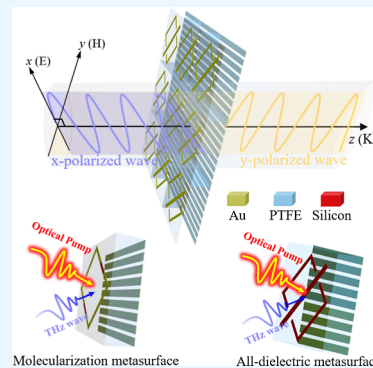
Read Online

ACCESS |

Metrics & More

Article Recommendations

ABSTRACT: With the development of ultrafast optics, all-optical control of terahertz wave modulation based on semiconductors has become an important technology of terahertz wave regulation. In this article, an ultrawideband terahertz linear polarization converter consisting of a double-layered metasurface is first proposed. The polarization conversion ratio of the device is $\sim 100\%$ at 0.2–2.2 THz, and the transmission of copolarization approaches zero in the full band, which demonstrates the ability of high-purity output with rotating input linear polarization of 90° over an ultrawideband. By analysis of the surface current and electric field distribution, the physical mechanism of polarization conversion is elucidated. In addition, the influence of important geometric parameters on the device is discussed and analyzed in detail, which provides theoretical support for the design of high-performance polarization converters. More importantly, by introducing semiconductor silicon to construct an actively controllable metasurface, we design all-optical polarization converters based on a meta-atomic molecularization metasurface and all-dielectric metasurface; the dynamically tunable ultrawideband linear polarization conversion is realized under optical pumping, which solves the inherent problem of the performance of the metasurface polarization converters. Numerical simulation shows that the switching response of the two types of actively controllable devices under optical pumping is about 700 and 1800 ps, respectively, and can manipulate polarized wave conversion ultrafast, which brings new opportunities for all-optical controlled ultrafast terahertz polarization converters. Our results provide a feasible scheme for the development of state-of-the-art active and controllable ultrafast terahertz metasurface polarization converters, which have great application potential in short-range wireless terahertz communication, ultrafast optical switches, the transient spectrum, and optical polarization control devices.



1. INTRODUCTION

Terahertz (THz) waves are an important branch of the electromagnetic (EM) spectrum, with frequencies ranging from 0.1 to 10 THz (1 THz = 10^{12} Hz). The unique advantages of terahertz waves make them an important research field in biology, medicine, materials science, information science, and spectroscopy.^{1,2} Polarization is one of the basic characteristics of EM waves, which plays a crucial role in terahertz functional devices, such as terahertz sensors, modulators, etc.^{3,4} Traditional polarization control devices rely on the anisotropic characteristics of the material's own structure, such as grating, birefringence effect, and dichroic crystal, which leads to its large volume, not easy integration, narrow bandwidth, low efficiency, high loss, and other defects. The unique physical properties (such as negative refractive index, negative permittivity, negative permeability, etc.) of the metasurface can effectively control the amplitude, phase, polarization, and transmission characteristics of terahertz waves, which provides an effective way for the realization of terahertz functional devices.^{5–7} In 2013, Chen et al. designed reflective and transmitted metasurface polarization converters based on stub arrays. For the reflection type, the bandwidth for polarization conversion ratio (PCR) above 84% is about 1

THz; for the transmission type, the PCR is above 55% at 0.52–1.82 THz.⁸ In 2014, Cheng et al.⁹ designed a reflective terahertz linear polarization converter with a top structure consisting of a double-open resonant ring and a metal disk. The PCR is $>50\%$ at 0.53–1.36 THz. Yang et al. proposed a polarization converter based on rectangular perforated graphene operating in the mid-infrared frequency band. Its operating frequency and PCR have significant tunable characteristics, but its relative bandwidth (RBW) with linear polarization conversion efficiency greater than 90% is only 5%.¹⁰ Xia et al. designed a linear polarization converter consisting of a metal patch array and a metal chiral metamaterial. At 0.73–1.41 THz, the PCR is above 95%.¹¹ Bilal et al. achieved perfect polarization conversion at 1.10 THz and 2.13 THz.¹²

Received: October 23, 2023
Revised: November 24, 2023
Accepted: November 28, 2023
Published: December 11, 2023



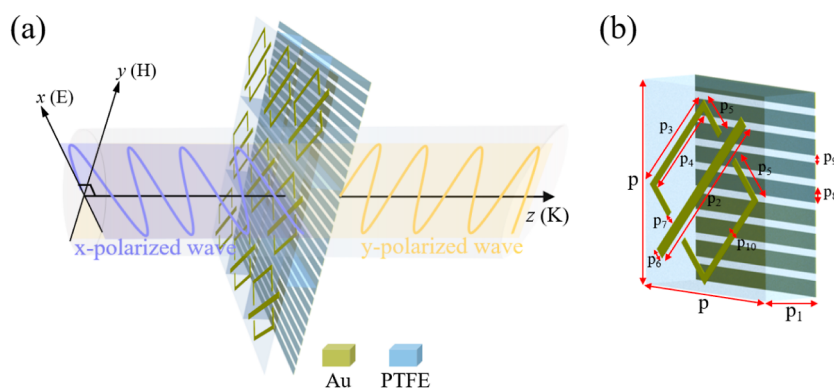


Figure 1. (a) The schematic diagram of the ultrawideband linear polarization converter and (b) the unit structure. The x , y , and z represent the coordinate axes. E , H , and K represent the electric field, magnetic field, and wave vector, respectively. Yellow represents gold (Au) with a conductivity of 4.56×10^7 S/m, which is a lossy metal. Blue represents PTFE with a dielectric constant of 2.1, and the dielectric dissipation factor ($\tan\delta$) is 0.001. The thickness of the top metal structure and the bottom metal CWA is $t = 0.2 \mu\text{m}$, the thickness of PTFE is $P_1 = 30 \mu\text{m}$, and the other geometric parameters are $P = 100 \mu\text{m}$, $P_2 = 100 \mu\text{m}$, $P_3 = 64 \mu\text{m}$, $P_4 = 56 \mu\text{m}$, $P_5 = 24 \mu\text{m}$, $P_6 = 6 \mu\text{m}$, $P_7 = 5 \mu\text{m}$, $P_8 = 8 \mu\text{m}$, $P_9 = 3.5 \mu\text{m}$, $P_{10} = 4 \mu\text{m}$.

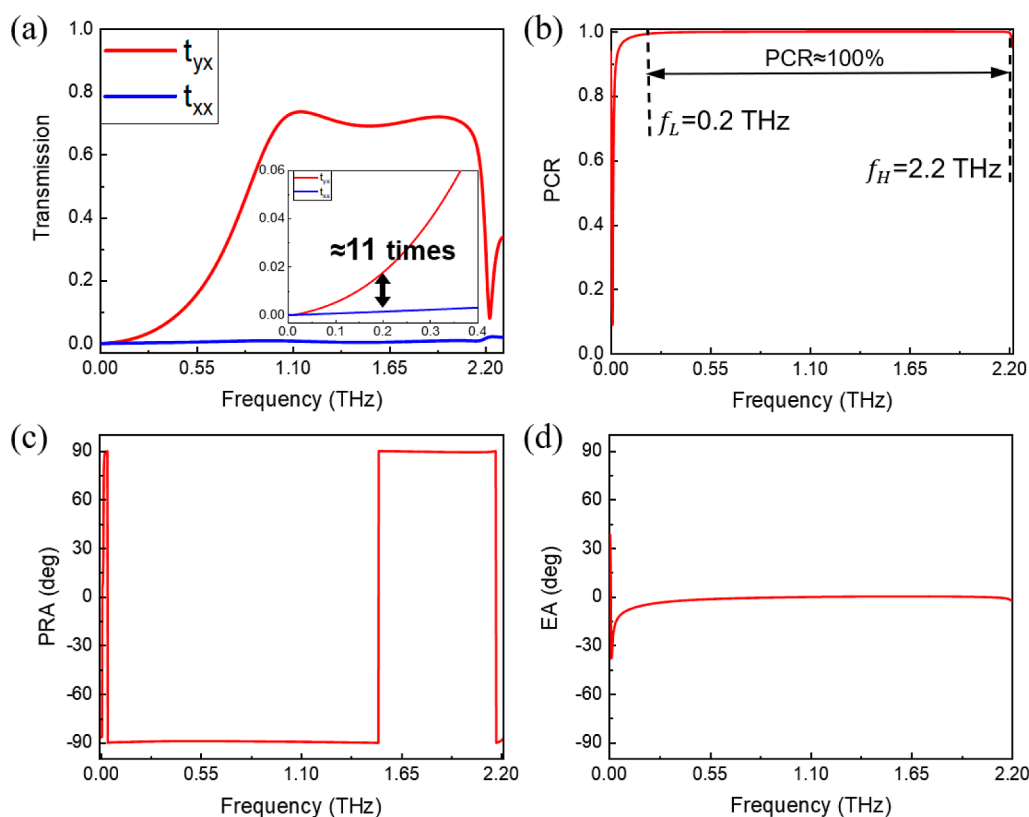


Figure 2. (a) Transmission of copolarization and cross-polarization for x -polarized incident waves, (b) PCR, (c) PRA, and (d) EA. The inset in Figure 2a shows a local magnification of the low-frequency band.

From the above research results, the performance of terahertz polarization converters in terms of polarization conversion bandwidth, PCR, and RBW needs to be further improved. To solve these problems, a polarization conversion device based on the Fabry-Pérot (F-P) cavity model is designed,^{8,13–15} in which each layer is equivalent to a mirror, and the interference of polarization couplings in a multi-reflection process may either enhance or reduce the overall emergent fields with co- and cross-polarization. Moreover, the performance of terahertz metasurface polarization converters could not be tunable or switchable after the design is completed, which greatly limits their application range and

flexibility. Therefore, active tunable materials can be introduced such as diodes,¹⁶ photosensitive silicon,^{17–20} liquid crystals,²¹ graphene,^{22–25} vanadium dioxide,^{26–29} etc. In terms of regulation modes, there are thermal, electrical, magnetic, light, mechanical, etc.^{30–37} Among them, for semiconductor materials, particularly high resistance (HR) silicon is suitable for all-optical modulation of terahertz waves by converting photons into electrons.³⁸ Silicon has the advantages of large carrier mobility, high absorption, and suitable energy band, and is widely used in various industries.^{39,40} As a result, silicon-based terahertz electronics have become the interface between silicon-based electronics and photonics for the realization of

terahertz functional devices or reconfigurable quasi-optical terahertz components.^{41,42}

In this article, an ultrawideband terahertz linear polarization converter consisting of a double-layered metasurface is first proposed. In the range of 0.2–2.2 THz, the PCR is close to 100%, the RBW is 166.7%, the polarization rotation angle (PRA) is $\sim 90^\circ$ (at 0.04–2.2 THz), and the ellipticity angle (EA) is $\sim 0^\circ$ (at 0.65–2.2 THz), which has a remarkable linear polarization transmission ability. The physical mechanism of polarization conversion is explained in detail by analyzing the current and electric field distribution. Moreover, two kinds of optically controlled terahertz polarization converters are designed by introducing silicon to construct an actively controllable metasurface. Numerical simulation shows that under femtosecond laser pulse modulation, the switching response time of the device is about 700 and 1800 ps, respectively, and it has the ultrafast modulation capability of picosecond order. This work provides a promising approach for the development of active and controllable terahertz metasurface polarization converters, which have a wide application prospect in terahertz high-speed optical communication, transient spectrum, ultrafast optical switches, optical polarization control devices, etc.

2. RESULTS AND DISCUSSION

2.1. Structure Design and Performance. The schematic diagram of the ultrawideband linear polarization converter is illustrated in Figure 1a. The x - z plane is the incident plane, the x -polarized incident wave is normal incidence (incident angle is 0° , degree of polarization is 1), and the metasurface linear polarization converter converts the x -polarized wave to a pure y -polarized wave. The unit structure consists of two metal layers and an intermediate medium layer, in Figure 1b. To show the actual performance of the device, the metal materials and media used are lossy materials. The top structure consists of a split-ring resonator (SRR) and cut-wire resonator (CWR), the bottom layer is composed of a metal cut-wire array (CWA), and the middle is a poly(tetrafluoroethylene) (PTFE) dielectric layer.

In order to further reflect the polarization conversion effect, the PCR can be calculated according to the transmission of copolarization and cross-polarization⁴³

$$\text{PCR} = t_{yx}^2 / (t_{yx}^2 + t_{xx}^2) \quad (1)$$

where the subscripts x and y represent two polarization states of the EM waves; yx (or xx) indicates that the polarization direction of EM waves changes from x to y (or x); the transmission of cross-polarization $t_{yx} = E_x^t / E_x^i$, the transmission of copolarization $t_{xx} = E_x^t / E_x^i$; superscripted i and t represent incident and transmitted EM waves, respectively. The transmission of cross-polarization, copolarization, and PCR for x -polarized normal incidence are shown in Figure 2a,b. The performance of the metasurface polarization converter is simulated based on the finite element method.

In Figure 2a, t_{yx} is above 0.6 at 0.93–2.16 THz, which means that the energy carried by cross-polarization transmission reaches more than 60% of the incident power. The transmission of copolarization approaches 0 at 0–2.2 THz (such as at 0.2 THz, t_{xx} is 0.0015; at 1.2 THz, t_{xx} is 0.0063; at 2 THz, t_{xx} is 0.0093), demonstrating the capability of rotating the input linear polarization by 90° with high output purity over an ultrawideband. For low-frequency bands, such as at 0.2

THz, the cross-polarization transmission capacity is 1 order of magnitude larger than the copolarization transmission capacity, which ensures the utilization efficiency of polarized waves in the low-frequency band. Thus, in the full band, the conversion from the x -polarized incident EM wave to the x -polarized wave is well suppressed, and the x -polarized wave to the pure y -polarized wave. There are two polarization conversion peaks, which are located at 1.145 THz ($t_{yx} = 0.74$, $t_{xx} = 0.0072$) and 1.93 THz ($t_{yx} = 0.72$, $t_{xx} = 0.0085$), respectively; polarization conversion valley at 1.535 THz ($t_{yx} = 0.69$, $t_{xx} = 0.0035$). In Figure 2b, the PCR is $\sim 100\%$ at 0.2–2.2 THz, which means that the polarization converter can convert an incident x -polarized wave to an almost complete y -polarized wave in the ultrawideband range.

For ultrawideband polarization converters, the RBW is usually used to quantitatively describe its broadband performance. The RBW is defined by

$$\text{RBW} = 2(f_H - f_L) / (f_H + f_L) \quad (2)$$

where f_H and f_L represent the upper and lower limits of the operating bandwidth of PCR close to 100%, respectively, and $f_H - f_L$ is the absolute bandwidth (ABW). Therefore, the PCR can maintain nearly 100% of the RBW up to $\sim 166.7\%$, and the ABW is 2 THz.

To accurately describe the transmitted EM wave, we introduced PRA and EA to determine the polarization state. The PRA and EA are defined as

$$\text{PRA} = \frac{1}{2} \tan^{-1} \left(\frac{2t_{xx}t_{yx} \cos \delta}{t_{xx}^2 - t_{yx}^2} \right) \quad (3)$$

$$\text{EA} = \frac{1}{2} \sin^{-1} \left(\frac{2t_{xx}t_{yx} \sin \delta}{t_{xx}^2 + t_{yx}^2} \right) \quad (4)$$

here $\delta = \varphi_y - \varphi_x$ is the phase difference of t_{yx} and t_{xx} . Figure 2c,d shows the PRA and EA of the incident EM waves for the x -polarization direction through the polarization converter. From Figure 2c, at 0.04–2.2 THz, the PRA is close to 90° , which indicates that the transmitted wave is approximately a linearly polarized wave perpendicular to the incident wave. In Figure 2d, the EA is less than 1° at 0.65–2.2 THz. The above results show that the metasurface linear polarization converter has the ability of high purity output with rotating input linear polarization of 90° over an ultrawideband. This means that the device can perfectly convert x -polarized incident waves into y -polarized waves in the ultrawideband frequency band.

In Figure 3, the electric fields of 0.5 and 2 THz incident x -polarized waves (E_x^i) and the electric fields after passing through the polarization converter are given (E_x^t). The color bars in the picture have been normalized. In Figure 3a,b, at 0.5 THz, the polarization direction of the incident x -polarized wave is the normal incidence, the polarization direction of the transmitted EM wave is vertical (y -polarized wave), and the polarization direction is rotated by 90° . At 2 THz, the electric field direction of the x -polarized wave is also rotated by 90° . The results show that the device has a good ability for linear polarization transmission.

2.2. Performance Comparison. To show the polarization conversion capability of the device, the polarization conversion bandwidth and PCR of different types of polarization converters are described in Table 1.^{8,9,11,26,44–50} The first polarization converter is designed in the article, the trans-

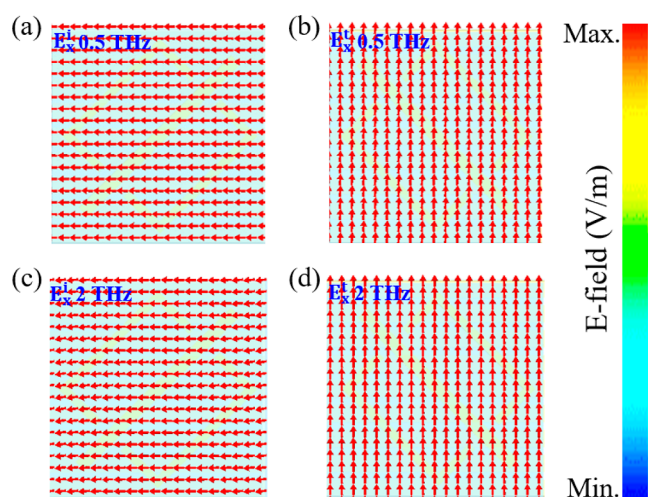


Figure 3. Electric field direction of EM waves at different frequencies. (a) E_x^i at 0.5 THz, (b) E_x^t at 0.5 THz, (c) E_x^i at 2 THz, and (d) E_x^t at 2 THz.

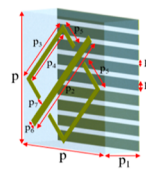
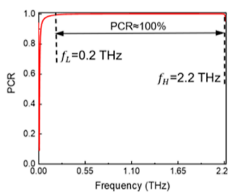
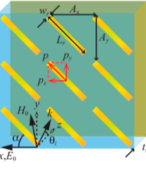
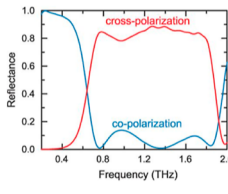
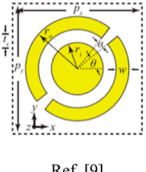
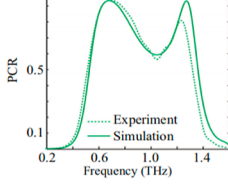
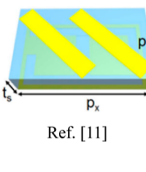
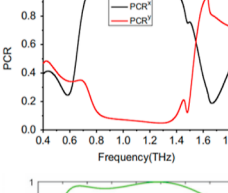
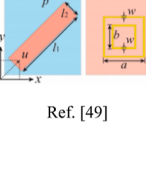
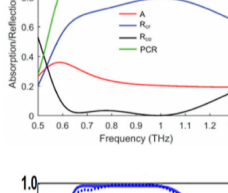
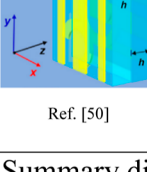
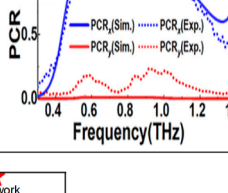
mission of cross-polarization is above 0.6 at 0.93–2.16 THz; the transmission of copolarization is close to 0 at 0–2.2 THz, and PCR is $\sim 100\%$ at 0.2–2.2 THz. In the second polarization converter, at 0.7 to 1.9 THz, the cross-polarized reflection is larger than 50%, and the copolarized component is mostly below 20%. The reflection of copolarization of the device fluctuates greatly, which indicates that the device cannot maintain the ideal polarization conversion. The efficiency can reach 84% and the spectrum width is about 1.0 THz. In addition, at 0.2–0.6 THz, the copolarized reflection is greater than the cross-polarized reflection, indicating that the cross-polarization conversion ability of the device is insufficient in the low-frequency band. The third polarization converter, the PCR is above 50% at 0.53–1.36 THz. For the fourth polarization converter, the PCR is above 95% at 0.73–1.41 THz; at 0.79 THz, the PCR is close to 100%. For the fifth polarization converter, the PCR is above 95% at 0.63–1.12 THz. In the sixth polarization converter, the PCR from 0.5 to 1.1 THz is close to 1, but the polarization conversion bandwidth is only 0.6 THz. For ref 26, at 0.58–1.4 THz, the PCR is maintained above 98%, but the polarization conversion bandwidth is narrow. For the ref 44, at 0.91–1.45 THz, the PCR is above 90%. To the PRA, the polarization rotation of 90° can only be maintained in a very narrow bandwidth range, so the linear transmission capability is not ideal. For ref 45, the PCR is larger than 70% in the range of 0.67–1.31 THz. However, the transmission of copolarization is not well suppressed. For ref 46, at 0.48–0.72 THz, the polarization of more than 90% of the incident electric field from the x direction to the y direction after reflected from the device. The performance of the above devices is visually expressed in the summary diagram in Table 1. The red stars show the results obtained from the article, indicating an improved performance among the polarization conversion bandwidth, PCR, and linear polarization transmission ability; hence, our device provides a feasible scheme for the design of high-performance ultrawideband linear polarization converters.

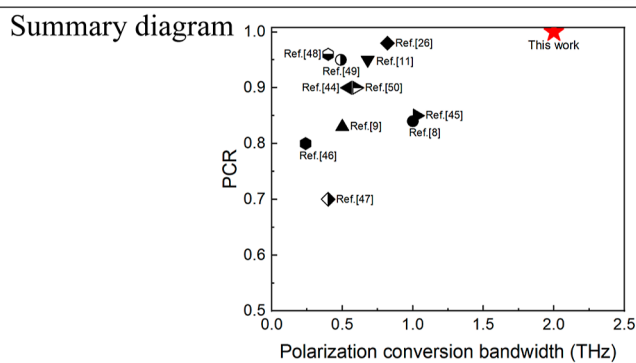
2.3. Analysis of the Polarization Conversion Mechanism. In order to further explore the physical mechanism of the ultrawideband metasurface polarization converter, the equivalent current distribution of the top metal structure and the bottom metal CWA were observed at three resonant

frequency points 1.145, 1.535, and 1.93 THz. The top metal structure and the bottom metal CWA of the unit structure can be regarded as the F-P-like cavity, which realizes the polarization conversion due to the multiple polarization coupling effect on the incident EM wave.^{8,43,51} In Figure 4a–c, at 1.145 THz, the component of the equivalent current of the top metal structure is opposite the bottom metal CWA. In this case, an equivalent ring current is formed between the top metal structure and the bottom metal CWA, which is equivalent to a magnetic dipole and generates magnetic resonance. The magnetic moment generated by the magnetic dipole will regulate the phase and amplitude of the EM wave and realize the conversion of cross-polarization. At 1.93 THz, the component of the equivalent current of the top metal structure is the same as that of the bottom metal CWA, then the top metal structure and the bottom metal CWA constitute an electric dipole and generate electrical resonance. The electric dipole moment generated by the electric dipole regulates the phase and amplitude of the EM wave to achieve cross-polarization conversion, as shown in Figure 4g–i. In Figure 4i, the direction of the electric dipole moment is the same as the direction of the electric field; that is, the direction of the electric dipole is the same direction as the electric field when the electric dipole is balanced in the electric field. At 1.535 THz, the equivalent current of the top metal structure and the bottom metal CWA have the same and opposite phenomena, and the magnetic dipole and the electric dipole are formed. The electric dipole moment generated by the electric dipole and the magnetic moment generated by the magnetic dipole jointly exert a regulatory effect on the EM wave, as shown in Figure 4d–f. Therefore, when the incident EM waves pass through the polarization converter, EM resonance is generated at different frequency points, and the magnetic moment or electric dipole moment formed has a regulatory effect on the EM waves so that the transmitted EM waves realize the change of polarization in ultrawideband frequency.^{52–54}

2.4. Polarization Conversion Properties for Various Parameters. Moreover, we analyzed the influence of the structural parameters on the polarization conversion performance, as shown in Figure 5. From Figure 5a,b, when the incident angle (θ) increases from 0 to 40° , the bandwidth of t_{yx} above 0.6 is decreased. It is worth noting that the amplitude corresponding to the t_{yx} peak hardly decreases with the increase in the incident angle, which means that the converter still has a strong polarization conversion ability to the x -polarized wave at a large incident angle. For example, when the incident angle is 20° , the maximal $t_{yx} = 0.753$ at 1.2 THz; when the incident angle is 40° , the maximal $t_{yx} = 0.805$ at 1.25 THz. In addition to several resonant frequency points, the PCR is close to 100% at 0.2–2.2 THz, and the ultrawideband polarization conversion can still be achieved. From the above data, the device has good incident angle stability, but with the increase of the oblique incident angle, the cross-polarization transmission bandwidth and PCR have adverse effects. The main reason is that when the incident angle of the incident x -polarized wave increases, its electric field component parallel to the surface of the structure will rapidly decrease, resulting in a decrease in the EM resonance intensity formed on the upper surface structure and the bottom metal CWA. In this case, the polarization conversion ability of the device caused by the F-P-like cavity model is reduced, resulting in a decrease in the broadband polarization conversion ability. In brief, as the

Table 1. Comparison of Performance Indicators of Polarization Conversion Bandwidth and PCR with Previous Reported Works^a

Structure of unit	Structural design	Operating frequency	PCR/Reflectance
	The top structure consists of metal SRR and CWR, the bottom layer is composed of metal CWA, and the middle is a PTFE dielectric layer.	0-2.2 THz	
This work			
	The unit structure consists of a metal CWA and a metal ground plane separated by a dielectric spacer.	0.2-2.4 THz	
Ref. [8]			
	A unit structure is composed of a metallic disk and SRR placed near to the ground plane and separated by a polydimethylsiloxane dielectric spacer.	0.2-1.6 THz	
Ref. [9]			
	The top layer is composed of two gold patches, and the bottom layer is made up of a planar chiral structure.	0.4-1.8 THz	
Ref. [11]			
	For the unit structure, from top to the bottom is VO ₂ brick-shaped antenna, a dielectric layer, double SRRs made of Cr, a continuous VO ₂ film, a second dielectric layer and a bottom Cr substrate.	0.5-1.3 THz	
Ref. [49]			
	It is composed of three metallic layers separated by two flexible polyimide dielectrics.	0.2-1.4 THz	
Ref. [50]			



^aReprinted with permission from ref 8 (Copyright 2013 American Association for the Advancement of Science); ref 9 (Copyright 2014 AIP Publishing); ref 11 (Copyright 2016 Elsevier B.V.); ref 49 (Copyright 2018 John Wiley & Sons); ref 50 (Copyright 2022 AIP Publishing).

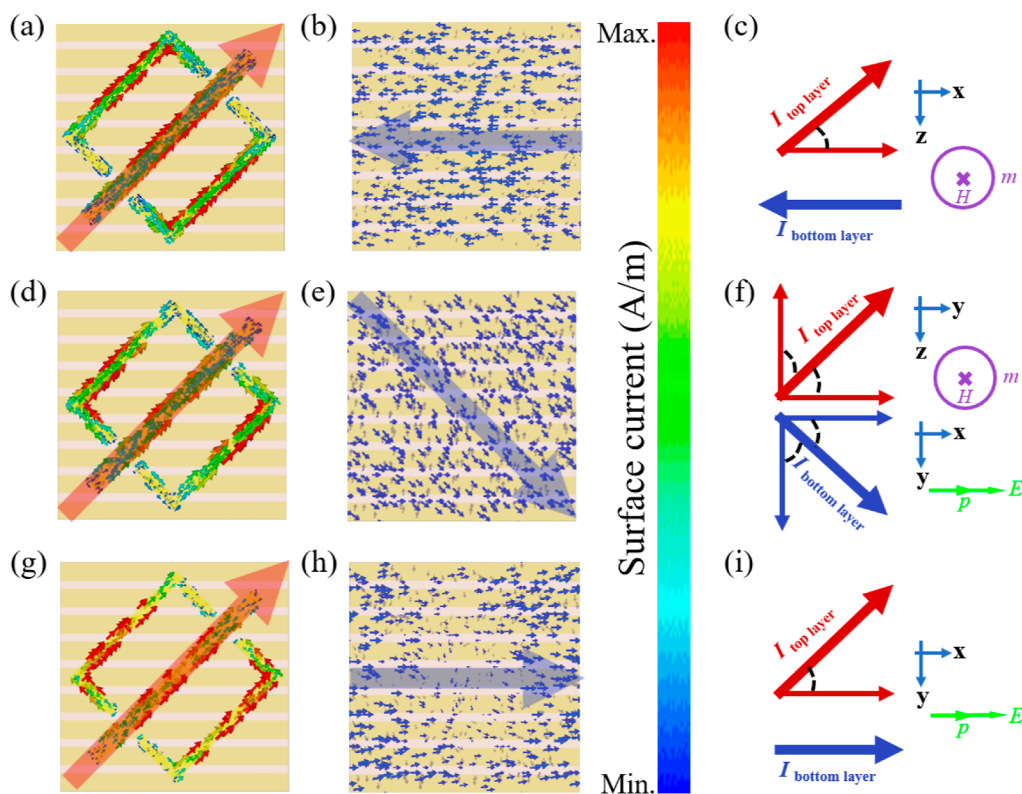


Figure 4. At 1.145 THz, the equivalent current of the top metal structure (a), the bottom metal CWA (b), and the resonance mode (c); at 1.535 THz, the equivalent current of the top metal structure (d), the bottom metal CWA (e), and the resonance mode (f); at 1.93 THz, the equivalent current of the top metal structure (g), the bottom metal CWA (h), and the resonance mode (i). The arrow direction is the direction of the equivalent current, m is the magnetic dipole, H (B , magnetic flux density) is the induced magnetic field, p is the electric dipole, and E is the induced electric field. The coordinate system is given in Figure 1. The color bars in the picture have been normalized.

incident angle continues to increase, the polarization direction of the incident terahertz wave changes; it is no longer a simple x -polarized wave, which no longer meets the polarization conversion conditions, and the polarization conversion ability of the device will further decline. In Figure 5c,d, when the dielectric constant (ϵ_r) of the intermediate dielectric layer (PTFE) is changed, the bandwidth of t_{yx} above 0.6 produces reduction and redshift. According to the EM metasurface regulation mechanism, the equivalent dielectric constant (ϵ_{eff}) and equivalent permeability (μ_{eff}) of the EM metasurface can be expressed as, respectively^{55,56}

$$\epsilon_{\text{eff}} = \frac{n_{\text{eff}}}{Z_{\text{eff}}} \quad (5)$$

$$\mu_{\text{eff}} = n_{\text{eff}} \cdot Z_{\text{eff}} \quad (6)$$

where n_{eff} is the equivalent refractive index and Z_{eff} is the equivalent wave impedance. According to eqs 5 and 6

$$n_{\text{eff}} = \sqrt{\epsilon_{\text{eff}} \cdot \mu_{\text{eff}}} \quad (7)$$

It can be seen from eq 7 that when the ϵ_r (or ϵ_{eff}) of the intermediate dielectric layer is changed, the n_{eff} of the device will change. Therefore, the change of ϵ_r affects the refractive index of the intermediate dielectric layer, and the EM response ability of the structure to the incident polarized wave shifts to the low frequency with the increase of ϵ_r (refractive index). It can be seen that when the ϵ_r is 5, the t_{yx} and the PCR both decrease significantly in the high-frequency band, but still maintain a high t_{yx} and the PCR in the low-frequency band. In Figure 5e,f, when the thickness of the intermediate dielectric

layer (PTFE, P_1) increases, the t_{yx} decreases with the increase of the thickness of the medium layer. This is due to the top metasurface structure and the bottom metal CWA of the polarization converter can be regarded as a structure similar to a resonator.^{55,56} When the thickness of the middle dielectric layer increases, the reflected energy of the EM wave will increase and the EM resonance intensity will weaken, resulting in a decrease of the t_{yx} . When $P_1 = 50 \mu\text{m}$, at 2.06 THz, PCR = 4.6%, and at 2.16 THz, PCR = 57%; when $P_1 = 60 \mu\text{m}$, at 1.72 THz, PCR = 14.2%. The above obvious resonance peak is because, when the frequency of the incident EM wave is just close to the resonant absorption frequency of the resonator, the cross-polarization transmission process will produce obvious ohmic loss and dielectric loss absorption. The multiple interference theory can also be used to explain that with the increase of the thickness of the intermediate dielectric layer, the F-P-like resonator structure can produce the interference effect of canceling or lengthening the EM wave of a specific frequency.^{57,58} In addition to the above several resonant frequency points, the device can maintain a high PCR in the ultrawideband frequency range. As can be seen from Figure 5g,h, changing the rotation angle of the top metal structure can control the polarization conversion and has an obvious switching effect. When the rotation angle is 45° , representing the position of the top metal structure in Figure 1; the rotation angle $\theta = 0^\circ$ indicates that the top metal structure is vertical; the rotation angle $\theta = 90^\circ$ indicates that the top metal structure is horizontal. When the rotation angle $\theta = 0^\circ$, at 0–2.2 THz, $t_{yx} = 0$, PCR = 0, the device can not realize the conversion of the x -polarized wave to the y -polarized wave. When the rotation

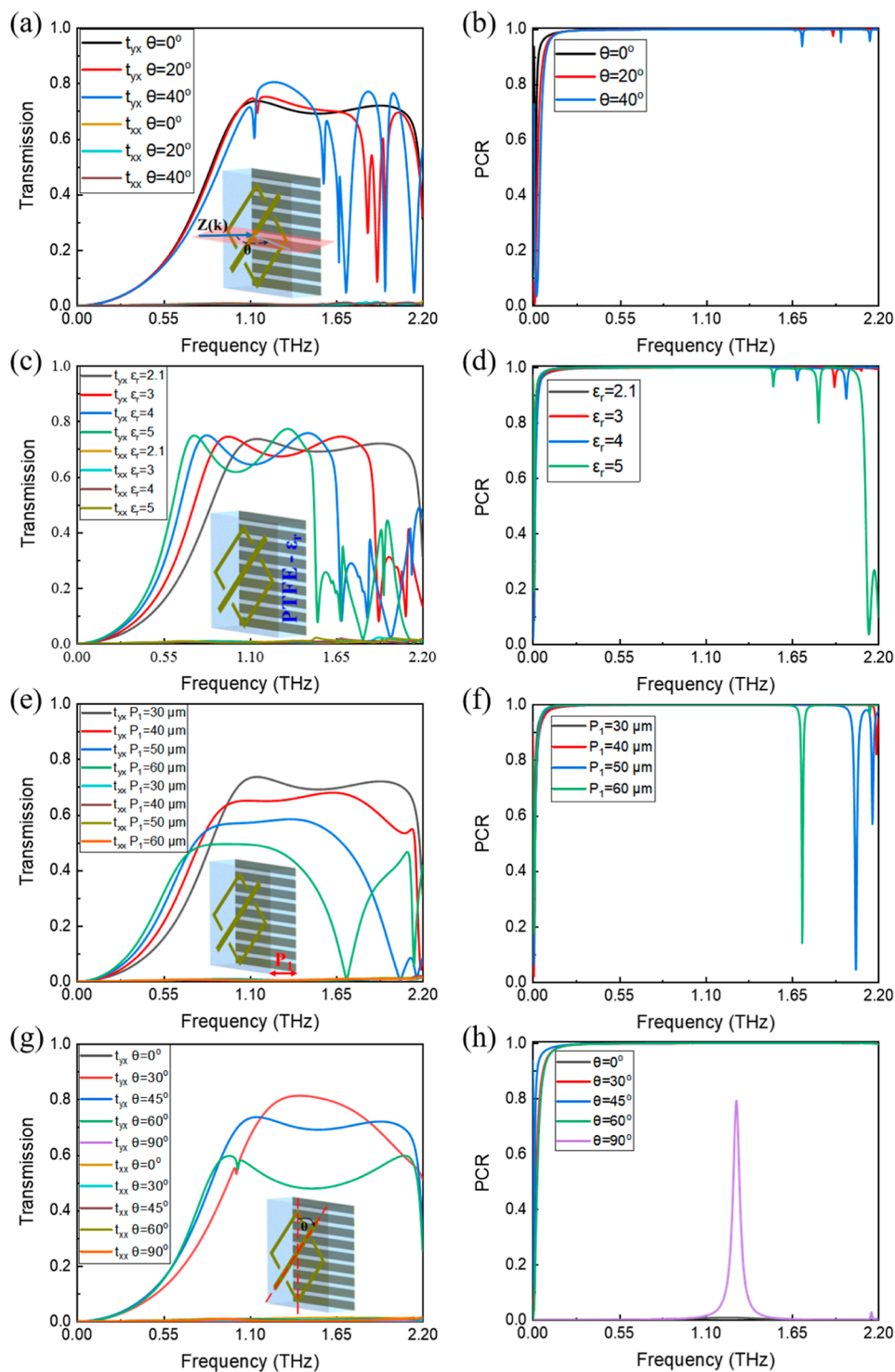


Figure 5. Influence of structural parameters on the polarization conversion performance. The influence of incident angle, (a) transmission of cross-polarization and copolarization, and (b) PCR. The dielectric constant, (c) transmission of cross-polarization and copolarization, and (d) PCR. The thickness of the intermediate dielectric layer, (e) transmission of cross-polarization and copolarization, and (f) PCR. The top metal structure rotation angle (clockwise rotation), (g) transmission of cross-polarization and copolarization, and (h) PCR.

angle $\theta = 30^\circ$, the t_{yx} reaches 81.4% at 1.42 THz. In the range 1.13–1.89 THz, the t_{yx} value is larger than 0.7. However, the bandwidth above 0.6 is narrower than that at 45° . When the rotation angle is 90° , at 0–2.2 THz, the t_{yx} is ~ 0 , and PCR is ~ 0 (at 1.3 THz, PCR = 80%), indicating that it is difficult for the device to realize the conversion of the x -polarized wave to y -polarized wave in the ultrawideband range at this time. From

the above data, the polarization conversion ability of the device can be controlled by the rotation angle of the top metal structure and the switching effect can be realized. This is because different rotation angles have different EM resonance capabilities for polarized EM waves, resulting in different cross-polarization capabilities and PCRs.

2.5. Optical-Controlled Polarization Conversion Metasurface.

2.5.1. Based on Meta-atomic Molecularization Metasurface. Combining terahertz metasurface with semiconductor materials may greatly promote the development of ultrafast terahertz polarization converters, which have great application potential in ultrawideband terahertz communication, terahertz imaging, and optical switching. However, the carrier dynamic process of semiconductor materials is generally constant without the action of the external excitation signal, so the modulation speed of the tunable terahertz polarization converter is single, which cannot meet the various applications in science and engineering. In this section, semiconductor silicon is first embedded in a specific location of the metasurface polarization converter. Silicon is a group IV element in the periodic table of chemical elements; each silicon atom has four valence electrons and silicon atoms are combined in a covalent bond to form crystals. Its crystal structure belongs to diamond, with a density of 10^{-3} kg/cm³, lattice constant 0.534 nm, melting point 1685 K, coefficient of thermal conductivity 1.56 W/(cm·K), band gap 1.12 eV (300 K), and intrinsic carrier concentration 1.02×10^{10} cm⁻³.⁵⁹ Benefiting from good carrier mobility, thermal conductivity, and suitable band gap, silicon has shown a wide range of applications in modern optoelectronics, including amplifiers, modulators, frequency converters, and optical switches.^{60,61} Based on the structure shown in Figure 1, the CWR is removed and the silicon is embedded in the gap of the SRR, as shown in Figure 6. The upper surface of the unit structure can be

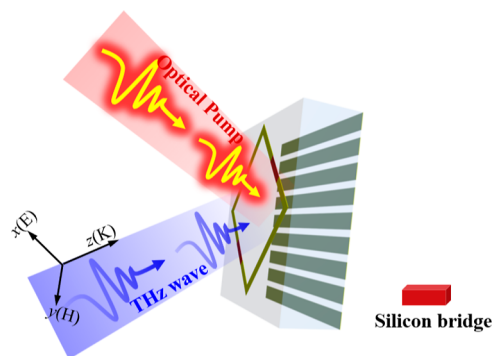


Figure 6. All-optical ultrawideband terahertz polarization converter based on meta-atomic molecularization metasurface. The incident terahertz waves refer to Figure 1. The size of the silicon bridge is $16 \times 4 \times 0.2$ μm , σ_{Si} is 0.25 S/m, and the dielectric constant is 11.9.

regarded as consisting of two meta-atoms connected by silicon bridges. Under optical pumping, when the incident photon energy is larger than the band gap of silicon, electrons transition through intrinsic absorption and produce a large number of photogenerated charge carriers (electron and hole pairs).⁵⁹ This work uses a pulsed laser of 800 nm to excite photogenerated charge carriers (e.g., amplified ~ 50 fs pulse width with a central wavelength of 800 nm or photon energy of 1.55 eV).^{35,62–65} Under optical pumping, the conductivity of silicon (σ_{Si}) can be actively regulated over a wide range, capable of reaching the order of 10^6 S/m.^{35,62,63,65–69} Therefore, with the increase of the pump power, the discrete SRR can be quickly conducted by exciting a large number of photocarriers in the silicon bridge, and the metasurface can be constructed from meta-atom to molecularization model, thus realizing ultrawideband polarization regulation.

Under optical pumping, the transmission of cross-polarization, the transmission of copolarization, and the PCR are shown in Figure 7. From Figure 7a, under femtosecond pulse laser modulation, the conductivity of the silicon bridge increases and the amplitude of t_{yx} gradually decreases. When σ_{Si} is 0.25–2.5 S/m, at 0.9–2.2 THz, t_{yx} is larger than 0.5; at 1.025–1.234 THz, t_{yx} is larger than 0.7; at 1.11 THz, the maximal t_{yx} is about 0.75. This state can be “switching on”. When σ_{Si} is 2.5×10^6 – 7.5×10^6 S/m, t_{yx} is close to 0 at 0–2.2 THz. This state can be “switching off.” It indicates that the x -polarized wave cannot be converted into a y -polarized wave after passing the polarization converter. In the process of optical pumping, t_{xx} is always close to 0, indicating that the device can well suppress the transmission of copolarization and ensure the transmission of pure y -polarized waves. With an increase in the pump power, the polarization conversion bandwidth decreases gradually. When σ_{Si} is 0.25 S/m, the PCR is close to 1 at 0.26–2.2 THz; when σ_{Si} is 7.5×10^6 S/m, the PCR is close to 1 at 1.136–1.226 THz, as shown in Figure 7b. When σ_{Si} is 0.25 S/m, the PRA is close to 90° at 0.18–2.2 THz; when σ_{Si} is 7.5×10^6 S/m, the bandwidth of PRA approaching 90° is only 0.11 THz (1.09–1.2 THz), as shown in Figure 7c. When σ_{Si} is 0.25 S/m, EA is close to 0° at 0.72–2.2 THz; when σ_{Si} is 7.5×10^6 S/m, the bandwidth of EA approaching 0° is only 0.31 THz (0–0.19 THz, 0.4–0.52 THz), as shown in Figure 7d. The above data show that the polarization converter can realize the mutual conversion between the cross-polarization mode and the copolarization mode under the condition of optical pumping and solve the inherent problem of the metasurface polarization converter. Figure 8 shows the distribution of the electric field intensity on the upper surface of the device at 1.11 THz. When σ_{Si} is 0.25 S/m, the electric field strength at the silicon bridge is very small, indicating that almost no current passes through and the SRR is in a state of not being connected. At this time, the equivalent current in the SRR has a fixed flow direction, and the bottom metal CWA can generate EM resonance, which can realize the polarization conversion of polarized waves, in Figure 8a. When σ_{Si} is 7.5×10^6 S/m (metal state), the electric field strength at the silicon bridge is large, indicating that there is a current through, and the SRR is in a connected state. The SRR has been equivalent to a metal ring, and the equivalent circulation formed by its current cannot generate a strong EM resonance with the bottom metal CWA, so the polarization conversion ability is weak, as shown in Figure 8b.

To study the ultrafast polarization conversion process of the silicon-based composite metasurface, the switching response of polarization conversion is measured by optical pump-terahertz probe (OPTP) measurements.^{70,71} The time for the pump pulse to reach the metasurface polarization converter is determined by the delay line of the pump light. Therefore, the switching response time can be defined as the time difference between the peak of the pump pulse and the peak of the terahertz pulse. To numerically simulate the dynamic evolution of the modulation spectrum, the photoexcited electron–hole density (N_{e-h}) evolving over time can be modeled using the following equation^{72,73}

$$\frac{dN_{e-h}}{dt} = -AN_{e-h} - BN_{e-h}^2 - CN_{e-h}^3 \quad (8)$$

$$\sigma(\omega) = \frac{\sigma_0}{1+i\omega\tau_d} \quad (9)$$

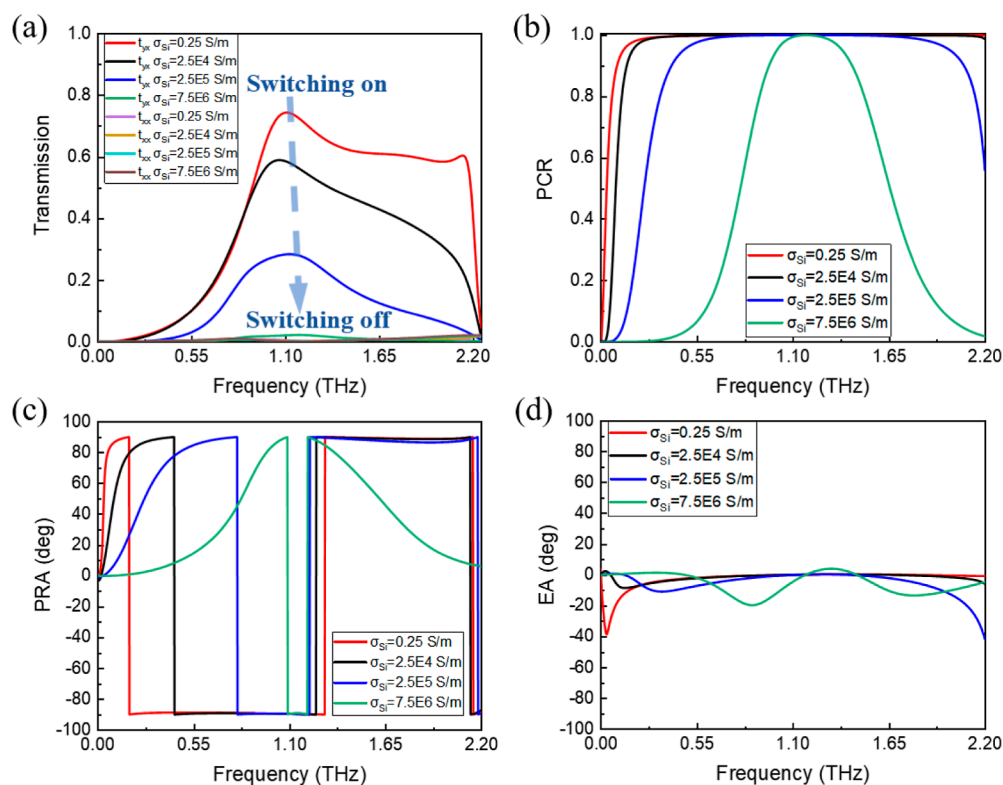


Figure 7. Transmission of cross-polarization and copolarization (a), PCR (b), PRA (c), and EA (d) of the polarization converter under optical pumping.

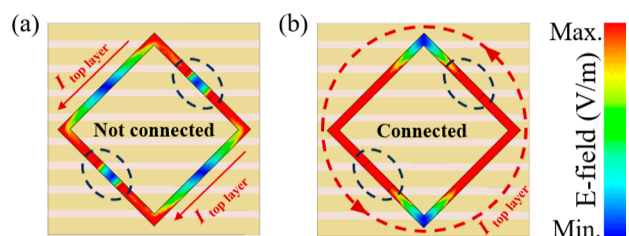


Figure 8. Electric field intensity of the unit structure at 1.11 THz under optical pumping, (a) 0.25 S/m and (b) 7.5×10^6 S/m.

where, A , B , and C are weighting factors for the monomolecular nonradiative decay, the radiative recombination decay, and the nonradiative Auger recombination decay, respectively; $\sigma(\omega)$ is the complex conductivity of the silicon bridge, σ_0 is the DC conductivity, ω is the angular frequency of THz waves, $\tau_d = 80$ fs is the Drude damping time. According to previous reports,^{71,74,75} the first-order recombination coefficient in silicon ranges from 2.65×10^9 s⁻¹ to 9.6×10^9 s⁻¹, the second-order recombination coefficient is 6×10^{-15} cm³ s⁻¹, and the third-order recombination coefficient is 3.8×10^{-31} cm⁶ s⁻¹. Combined with the Drude model, the change of complex conductivity caused by the photocarrier concentration can be determined. Under the excitation of a femtosecond pulse laser, the photocarrier concentration in the silicon bridge is significantly increased, and when the σ_{si} reaches 7.5×10^6 S/m, the discrete SRR is quickly conducted. The silicon bridge with high conductivity makes the upper surface of the unit structure be constructed from atomic to molecular model, which affects the EM resonance intensity of the polarization converter to realize the change of the polarization conversion ability. The OPTP measurement scheme is used to simulate

the transient evolution of polarization conversion as shown in Figure 9a. Figure 9b shows the transient electric field spectra monitored by the pump–probe with various time delays when the silicon bridge conductivity reaches 7.5×10^6 S/m. When the time delay is 700–900 ps, the transient electric field waveform is almost not changed, indicating that the switching response time for polarization conversion is about 700 ps. The photocontrolled switching time mainly depends on the relaxation time of the photocarriers in the silicon bridge. To realize the ultrafast active regulation of polarized waves, the photocarriers lifetime in the silicon bridge can be shortened by the injection of additional ions (such as phosphorus ions, and boron ions), and the polarization modulation speed of the terahertz metasurface can be further improved.^{76–78} Figure 9c shows the ultrafast modulation of the transient evolution of polarization conversion under a femtosecond pulse laser. At 0 ps, due to the large number of photocarriers generated in the silicon bridge, the split resonant ring is quickly connected into a whole structure under optical pumping, and the polarization conversion ability weakens rapidly. Therefore, “0 ps” can be considered as a state in which polarization conversion is “switching off”. With the increase of the time delay of a pulsed laser, the polarization conversion ability increases rapidly. When the pump pulse time delay reaches 700 ps, the metasurface recovers the ability of ultrawideband polarization conversion, that is, in the time delay of 700 ps, the metasurface polarization conversion ability can return to the state of no excitation. “700 ps” can be considered as the state in which polarization conversion is “switching on”. Figure 9c depicts the ultrafast tuning process of the polarization conversion, and the entire switching cycle can be completed in 700 ps. The above phenomenon occurs because the conductivity in the silicon bridge is weakened by photocarriers recombination, the

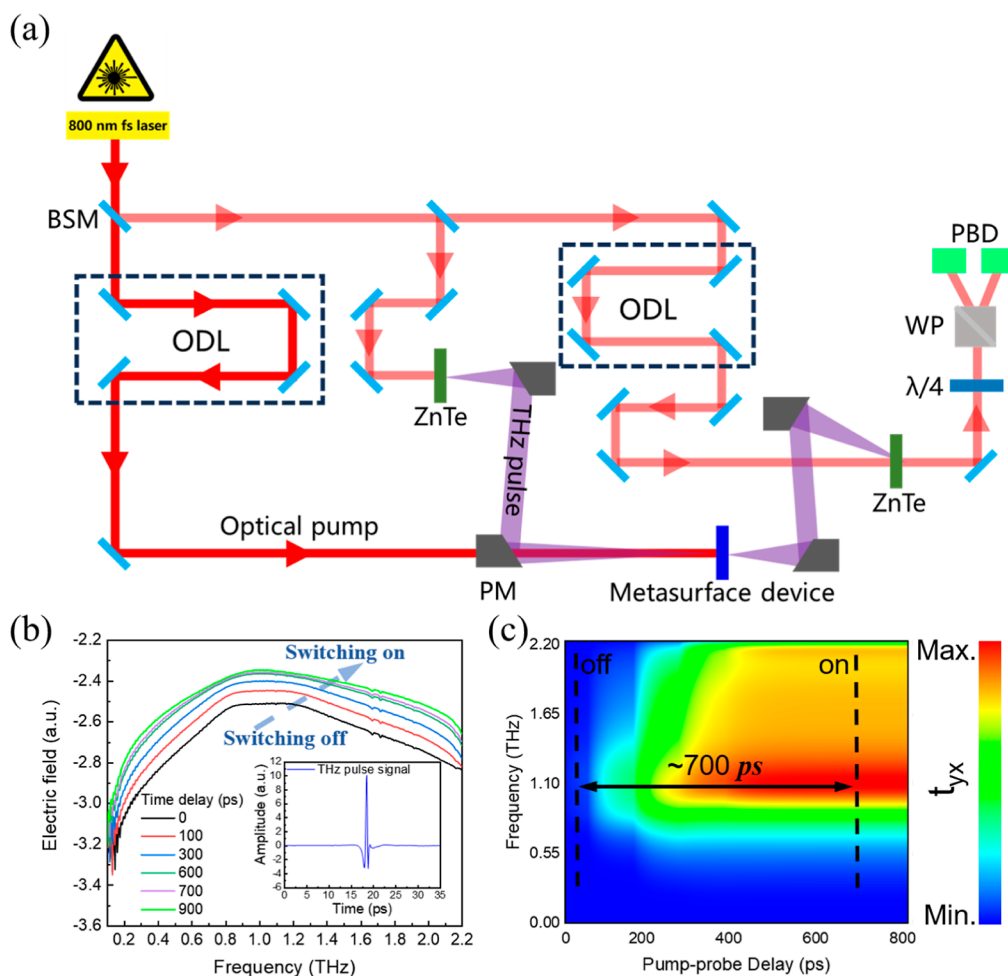


Figure 9. (a) Schematic diagram of a time-domain spectral system for optically pumped terahertz detection. BS: beam splitter mirror, ODL: optical delay line, PM: parabolic mirror, WP: Wollaston Prism; $\lambda/4$: quarter wave plate, PBD; photoelectric balance detector, ZnTe: zinc telluride crystal. The optical laser beam had a pulse width of ≈ 50 fs and a center wavelength of 800 nm with a 1 KHz repetition rate. (b) Transient electric field spectra are monitored by a pump–probe with various time delays. (c) Polarization conversion spectra map showing the transient switching dynamics for various pump–probe time delays. The conductivity of silicon is 7.5×10^6 S/m. The dotted line position of the bidirectional arrow indicates that the recovery time of the polarization conversion switch is about 700 ps.

molecular state cannot be maintained, and the unit structure is resplit into two meta-atoms. The ultrafast modulation of polarization conversion is realized through the molecularization of meta-atoms by optical pumping, which provides a new research idea for ultrafast terahertz polarization converters based on metasurface.

In this section, by reasonably designing a hybrid metasurface and using external photoexcitation to control the physical state of the silicon bridge, the meta-atom to molecularization model is constructed, and the ultrafast regulation of polarization conversion devices is realized, which has great application potential in the fields of ultrawideband communication, photocontrolled switching, and transient spectroscopy.

2.5.2. Based on All-Dielectric Metasurface. This section replaces the metal SRR and CWR in Figure 1 with the SRR and CWR based on semiconductor silicon. The unit structure is shown in Figure 10. The tunable polarization conversion performance of the device is also studied under external photoexcitation.

Under optical pumping, the transmission of cross-polarization, the transmission of copolarization, and the PCR are shown in Figure 11. From Figure 11a, the transmission of cross-polarization gradually increases with the increase of the

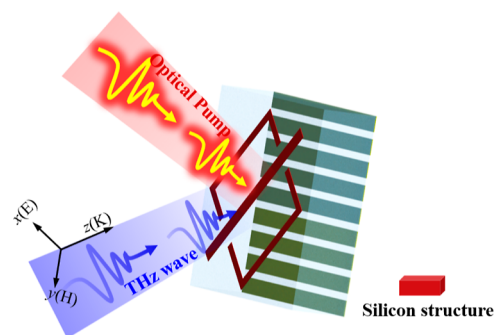


Figure 10. All-optical ultrawideband terahertz polarization converter based on all-dielectric metasurface. The incident terahertz waves refer to Figure 1. The σ_{Si} is 0.25 S/m, and the dielectric constant is 11.9.

intensity of the optical pumping; but the transmission of copolarization is always close to 0, which ensures the pure polarized wave transmission. When σ_{Si} is 0.25 S/m, t_{yx} is ~ 0 , indicating that the incident x -polarized wave is not able to be converted into a y -polarized transmitted wave after passing through the polarization converter; at this time, the PCR is 0, as shown in Figure 11b. This state can be “switching off.”

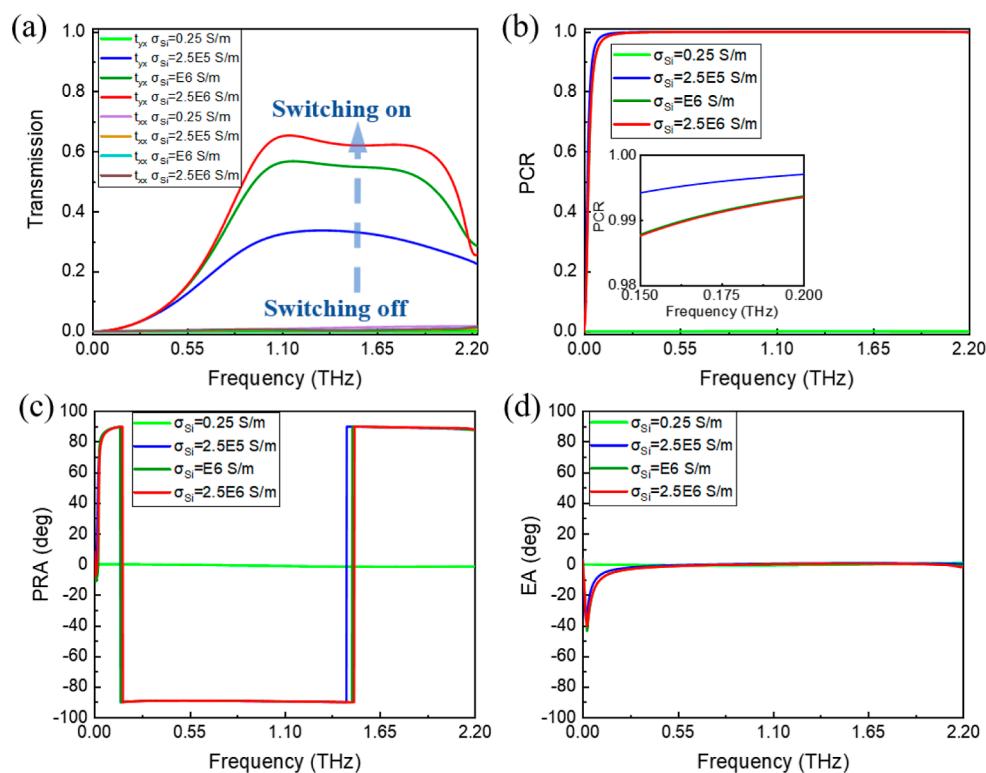


Figure 11. Transmission of cross-polarization and copolarization (a), PCR (b), PRA (c), and EA (d) of the polarization converter under optical pumping.

When σ_{Si} is 2.5×10^6 S/m, the t_{yx} is larger than 0.6 at 0.796–1.94 THz, and the maximal $t_{yx} = 0.66$ at 1.14 THz; the PCR reaches $\sim 100\%$ at 0.2–2 THz. This state can be “switching on.” Therefore, under optical pumping, the incident polarized wave can be switched between the copolarized mode and the cross-polarized mode, which realizes the optically controlled tunability of the PCR and polarization conversion bandwidth. The reason the device achieves optically controlled tunable polarization conversion is explained in Figure 12. The color

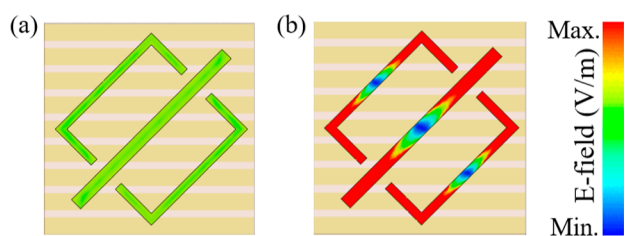


Figure 12. Electric field intensity of the top structure at 1.14 THz under optical pumping, (a) 0.25 S/m and (b) 2.5×10^6 S/m.

bars in the picture have been normalized. Under the optical pumping, the photogenerated carrier concentration in silicon will be increased, and the top structure will be transformed from a semiconductor state to a metal state, thus realizing the electrical resonance or magnetic resonance of the top surface structure and the bottom CWA, and completing the polarization conversion. Therefore, Figure 12a,b shows the electric field intensities in the top layer of 1.14 THz under different optical pumping intensities to show the concentration of photogenerated carriers and the strength of EM resonance. When σ_{Si} is 0.25 S/m, the surface electric field strength of the device is much lower than that when σ_{Si} is 2.5×10^6 S/m. It is

proved that under optical pumping, the device achieves polarization conversion by reconstructing EM resonance and exhibits a remarkable optical switching effect. To describe the polarization characteristics of the transmitted EM waves, the PRA and EA of the incident EM waves for the x -polarization direction through the polarization converter under optical excitation are shown in Figure 11c,d. When σ_{Si} is 0.25 S/m, the PRA = 0° and EA = 0° at 0–2.2 THz, and the incident x -polarized wave cannot be converted into the y -polarized wave. When σ_{Si} is 2.5×10^6 S/m, PRA is $\sim 0^\circ$ at 0.164–2.2 THz; at 0.6–2.2 THz, EA is $\sim 0^\circ$. The above data show that the device can realize a dynamic tunable linear polarization converter in the ultrawideband range under femtosecond laser modulation.

The ultrafast transient evolution of the polarization conversion is simulated under optical modulation by the OPTP method in Figure 9a. Figure 13a shows the transient electric field spectra monitored by the pump–probe with various time delays when σ_{Si} reaches 2.5×10^6 S/m. When the metasurface of silicon is excited by a femtosecond laser, many free carriers are generated in silicon, which realizes the metasurface transformation from semiconductor state to metal state, and thus, the polarization conversion is controlled. When the time delay reaches 1800 ps, the transient electric field of the terahertz wave does not change, indicating that the switching response time is about 1800 ps. Figure 13b shows the transient dynamic evolution process of polarization conversion under femtosecond laser pulse modulation. At 0 ps, the silicon with high conductivity and the bottom metal CWA produce strong EM resonance, resulting in strong polarization conversion ability. “0 ps”, can be considered as a state in which polarization conversion is “switching on.” With the increase in the time delay of the pulsed laser, the polarization conversion ability decreases gradually. When the

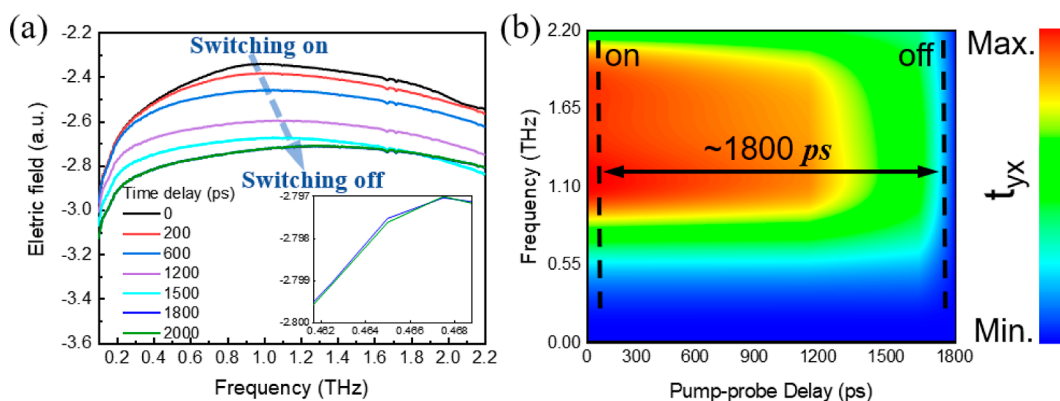


Figure 13. (a) Transient electric field spectra are monitored by a pump–probe with various time delays. (b) Polarization conversion spectra map showing the transient switching dynamics for various pump–probe time delays. The conductivity of silicon is 2.5×10^6 S/m. The dotted line position of the bidirectional arrow indicates that the recovery time of the polarization conversion switch is about 1800 ps.

time delay reaches 1800 ps, the device has almost no polarization conversion transmission capability. “1800 ps”, can be considered as a state in which polarization conversion is “switching off.” This shows that the polarization conversion ability can be restored to the state without optical excitation after a time delay of 1800 ps. This is due to photocarriers recombination in silicon that causes the conductivity to weaken and return to the semiconductor state. Figure 13b graphically shows the modulation process of polarization conversion, and the whole switching cycle can be completed within 1800 ps, which has the ability of ultrafast tuning of polarization conversion.

The above analysis shows that under the excitation of a femtosecond laser, due to the ultrashort relaxation time of photocarriers in silicon materials, the silicon-based metasurface has ultrafast optical switching characteristics and achieves ultrafast and ultrawideband optically controlled terahertz polarization conversion. The realization of ultrafast all-optical terahertz modulation by a semiconductor composite metasurface provides a new idea for the development of reconfigurable metasurface devices and brings new opportunities for the development of all-optical controlled ultrafast terahertz modulators.

3. CONCLUSIONS

In this work, we have demonstrated an ultrawideband terahertz linear polarization converter consisting of a double-layered metasurface. The PCR of the device is $\sim 100\%$ at 0.2–2.2 THz, the PRA is close to 90° at 0.04–2.2 THz and the EA is close to 0° at 0.65–2.2 THz, which has a strong linear polarization transmission ability. The physical mechanism of polarization conversion is elucidated by numerical simulation of the surface current and electric field distribution. The influence of geometric parameters on the performance of polarization converters is discussed and explained in detail, which has important guiding significance for the design of high-performance polarization converters. Importantly, the dynamic switching ultrawideband linear polarization converter is realized by introducing photosensitive silicon to reconstruct the EM resonance under optical pumping, which solves the inherent problem of the function of the metasurface polarization converter. Numerical simulation shows that the all-optical polarization converters based on meta-atomic molecularization metasurface and all-dielectric metasurface can achieve a switching response of about 700 and 1800 ps,

respectively, which brings a new opportunity for all-optical controlled ultrafast terahertz polarization conversion devices. Our results offer a feasible scheme for the development of active and controllable ultrawideband terahertz metasurface linear polarization converters, which have significant potential use for terahertz wireless communication, transient spectrum, ultrafast optical switches, optical polarization control devices, etc.

AUTHOR INFORMATION

Corresponding Author

Zhiming Huang – State Key Laboratory of Infrared Physics, Shanghai Institute of Technical Physics, Chinese Academy of Sciences, Shanghai 200083, P. R. China; University of Chinese Academy of Sciences, Chinese Academy of Sciences, Beijing 100049, P. R. China; Hangzhou Institute for Advanced Study, University of Chinese Academy of Sciences, Hangzhou 310024, P. R. China; Institute of Optoelectronics, Fudan University, Shanghai 200438, P. R. China; Key Laboratory of Space Active Opto-Electronics Technology, Shanghai Institute of Technical Physics, Chinese Academy of Sciences, Shanghai 200083, P. R. China; School of Microelectronics, Shanghai University, Shanghai 201800, P. R. China; Email: zmhuang@mail.sitp.ac.cn

Authors

Qiangguo Zhou – State Key Laboratory of Infrared Physics, Shanghai Institute of Technical Physics, Chinese Academy of Sciences, Shanghai 200083, P. R. China; University of Chinese Academy of Sciences, Chinese Academy of Sciences, Beijing 100049, P. R. China; orcid.org/0000-0002-3989-6655

Qinxi Qiu – State Key Laboratory of Infrared Physics, Shanghai Institute of Technical Physics, Chinese Academy of Sciences, Shanghai 200083, P. R. China; orcid.org/0000-0002-7044-7911

Tuntan Wu – State Key Laboratory of Infrared Physics, Shanghai Institute of Technical Physics, Chinese Academy of Sciences, Shanghai 200083, P. R. China; University of Chinese Academy of Sciences, Chinese Academy of Sciences, Beijing 100049, P. R. China; orcid.org/0000-0002-7640-4453

Yongzhen Li – State Key Laboratory of Infrared Physics, Shanghai Institute of Technical Physics, Chinese Academy of Sciences, Shanghai 200083, P. R. China; University of

Chinese Academy of Sciences, Chinese Academy of Sciences, Beijing 100049, P. R. China

Complete contact information is available at:

<https://pubs.acs.org/10.1021/acsomega.3c08355>

Notes

The authors declare no competing financial interest.

ACKNOWLEDGMENTS

We would like to thank Dr. Y. Hu and Dr. W. He for their support and assistance in the analysis of ultrafast carrier dynamics evolution. This work was supported by the National Science Funds (grant nos. 12134016, 61625505, and 62305361), Chinese Academy of Sciences (grant no. ZDBS-LY-JSC025), Sino-Russia International Joint Laboratory of Terahertz Materials and Devices (grant no. 18590750500), Shanghai Municipal Science and Technology Major Project (grant no. 2019SHZDZX01), and Shanghai Municipal Science and Technology Yangfan Special Project (grant no. 23YF145S300).

REFERENCES

- (1) Tonouchi, M. Cutting-edge terahertz technology. *Nat. Photonics* **2007**, *1*, 97–105.
- (2) Zhou, Q.; Qiu, Q.; Huang, Z. Graphene-based terahertz optoelectronics. *Opt. Laser Technol.* **2023**, *157*, 108558.
- (3) Huang, C.; Wang, Q.; Yin, X.; Zhang, Y.; Li, J.; Zhu, Y. Break Through the Limitation of Malus' Law with Plasmonic Polarizers. *Adv. Opt. Mater.* **2014**, *2*, 723–728.
- (4) Zhou, Q.; Li, Y.; Li, Y.; Yao, N.; Huang, Z. High efficiency of broadband transmissive metasurface terahertz polarization converter. *Chinese Phys. B* **2023**, *32*, 024201.
- (5) Pendry, J. B.; Holden, A. J.; Stewart, W. J.; Youngs, I. I. Extremely low frequency plasmons in metallic mesostructures. *Phys. Rev. Lett.* **1996**, *76*, 4773–4776.
- (6) Veselago, V. G. The electrodynamics of substances with simultaneously negative values of ϵ and μ . *Physics Uspekhi* **1968**, *10*, 509–514.
- (7) Parazzoli, C. G.; Greigor, R. B.; Li, K.; Koltenbah, B. E. C.; Tanielian, M. Experimental Verification and Simulation of Negative Index of Refraction Using Snell's Law. *Phys. Rev. Lett.* **2003**, *90*, 107401.
- (8) Grady, N. K.; Heyes, J. E.; Chowdhury, D. R.; Zeng, Y.; Reiten, M. T.; Azad, A. K.; Taylor, A. J.; Dalvit, D. A. R.; Chen, H. Terahertz metamaterials for linear polarization conversion and anomalous refraction. *Science* **2013**, *340*, 1304–1307.
- (9) Cheng, Y. Z.; Withayachumnankul, W.; Upadhyay, A.; Headland, D.; Nie, Y.; Gong, R. Z.; Bhaskaran, M.; Sriram, S.; Abbott, D. Ultrabroadband reflective polarization converter for terahertz waves. *Appl. Phys. Lett.* **2014**, *105*, 181111.
- (10) Yang, C.; Luo, Y.; Guo, J.; Pu, Y.; He, D.; Jiang, Y.; Xu, J.; Liu, Z. Wideband tunable mid-infrared cross polarization converter using rectangle-shape perforated graphene. *Opt. Express* **2016**, *24*, 16913–16922.
- (11) Xia, R.; Jing, X.; Zhu, H.; Wang, W.; Tian, Y.; Hong, Z. Broadband linear polarization conversion based on the coupling of bilayer metamaterials in the terahertz region. *Opt. Commun.* **2017**, *383*, 310–315.
- (12) Bilal, R. M. H.; Baqir, M. A.; Choudhury, P. K.; Ali, M. M.; Rahim, A. A. On the specially designed fractal metasurface-based dual-polarization converter in the THz regime. *Results Phys.* **2020**, *19*, 103358.
- (13) Sun, Y.; Gao, C.; Qu, J.; Zhang, H. Circularly Polarized Manipulations with VO₂-Doped Dielectric Electromagnetically Induced Transparency and Absorption. *Annalen der Physik* **2022**, *534*, 2200130.
- (14) Sun, Y.; Zhang, D.; Zhang, H. Tailoring dual-band electromagnetically induced transparency with polarization conversions in a dielectric-metal hybrid metastructure. *Opt. Express* **2022**, *30*, 30574–30591.
- (15) Cong, L.; Cao, W.; Zhang, X.; Tian, Z.; Gu, J.; Singh, R.; Han, J.; Zhang, W. A perfect metamaterial polarization rotator. *Appl. Phys. Lett.* **2013**, *103*, 171107.
- (16) Wang, J.; Yang, R.; Ma, R.; Tian, J.; Zhang, W. Reconfigurable Multifunctional Metasurface for Broadband Polarization Conversion and Perfect Absorption. *IEEE Access* **2020**, *8*, 105815–105823.
- (17) Zhao, X.; Lou, J.; Xu, X.; Yu, Y.; Wang, G.; Qi, J.; Zeng, L.; He, J.; Liang, J.; Huang, Y.; Zhang, D.; Chang, C. Multifield Controlled Terahertz Modulator Based on Silicon-Vanadium Dioxide Hybrid Metasurface. *Adv. Opt. Mater.* **2022**, *10*, 2102589.
- (18) Zhou, Q.; Li, Y.; Wu, T.; Qiu, Q.; Duan, J.; Jiang, L.; Mao, W.; Yao, N.; Huang, Z. Terahertz Metasurface Modulators Based on Photosensitive Silicon. *Laser Photon. Rev.* **2023**, *17*, 2200808.
- (19) Forouzmand, A.; Mosallaei, H. Electro-optical Amplitude and Phase Modulators Based on Tunable Guided-Mode Resonance Effect. *ACS Photonics* **2019**, *6*, 2860–2869.
- (20) Shi, Z.; Cao, X.; Wen, Q.; Wen, T.; Yang, Q.; Chen, Z.; Shi, W.; Zhang, H. Terahertz Modulators Based on Silicon Nanotip Array. *Adv. Opt. Mater.* **2018**, *6*, 1700620.
- (21) Dolan, J. A.; Cai, H. G.; Delalande, L.; Li, X.; Martinson, A.; de Pablo, J. J.; Lopez, D.; Nealey, P. F. Broadband Liquid Crystal Tunable Metasurfaces in the Visible: Liquid Crystal Inhomogeneities Across the Metasurface Parameter Space. *ACS Photonics* **2021**, *8*, 567–575.
- (22) Zhang, Y.; Feng, Y.; Jiang, T.; Cao, J.; Zhao, J.; Zhu, B. Tunable broadband polarization rotator in terahertz frequency based on graphene metamaterial. *Carbon* **2018**, *133*, 170–175.
- (23) Padmanabhan, P.; Boubanga-Tombet, S.; Fukidome, H.; Otsuji, T.; Prasankumar, R. P. A graphene-based magnetoplasmonic metasurface for actively tunable transmission and polarization rotation at terahertz frequencies. *Appl. Phys. Lett.* **2020**, *116*, 221107.
- (24) Li, G.; Wang, G.; Yang, T.; Zhang, Y.; Shen, J.; Zhang, B. Graphene-based terahertz bias-driven negative-conductivity metasurface. *Nanoscale Adv.* **2022**, *4*, 3342–3352.
- (25) Chen, X.; Tian, Z.; Lu, Y.; Xu, Y.; Zhang, X.; Ouyang, C.; Gu, J.; Han, J.; Zhang, W. Electrically Tunable Perfect Terahertz Absorber Based on a Graphene Salisbury Screen Hybrid Metasurface. *Adv. Opt. Mater.* **2020**, *8*, 1900660.
- (26) Luo, J.; Shi, X.; Luo, X.; Hu, F.; Li, G. Broadband switchable terahertz half-/quarter-wave plate based on metal-VO₂ metamaterials. *Opt. Express* **2020**, *28*, 30861–30870.
- (27) Qi, L. M.; Liu, C.; Zhang, X.; Sun, D. D.; Shah, S. Structure-insensitive switchable terahertz broadband metamaterial absorbers. *Appl. Phys. Express* **2019**, *12*, 062011.
- (28) Li, X.; Tang, S.; Ding, F.; Zhong, S.; Yang, Y.; Jiang, T.; Zhou, J. Switchable multifunctional terahertz metasurfaces employing vanadium dioxide. *Sci. Rep.* **2019**, *9*, 5454.
- (29) Peng, Z.; Zheng, Z.; Yu, Z.; Lan, H.; Zhang, M.; Wang, S.; Li, L.; Liang, H.; Su, H. Broadband absorption and polarization conversion switchable terahertz metamaterial device based on vanadium dioxide. *Opt. Laser Technol.* **2023**, *157*, 108723.
- (30) Jung, H.; Jo, H.; Lee, W.; Kang, M. S.; Lee, H. Reconfigurable Molecularization of Terahertz Meta-Atoms. *ACS Photonics* **2022**, *9*, 1814–1820.
- (31) Jung, H.; Koo, J.; Heo, E.; Cho, B.; In, C.; Lee, W.; Jo, H.; Cho, J. H.; Choi, H.; Kang, M. S.; Lee, H. Electrically Controllable Molecularization of Terahertz Meta-Atoms. *Adv. Mater.* **2018**, *30*, 1802760.
- (32) Xu, Z.; Lin, Y. A Stretchable Terahertz Parabolic-Shaped Metamaterial. *Adv. Opt. Mater.* **2019**, *7*, 1900379.
- (33) Zhao, Y. C.; Wang, L.; Zhang, Y. X.; Qiao, S.; Liang, S. X.; Zhou, T. C.; Zhang, X. L.; Guo, X. Q.; Feng, Z. H.; Lan, F.; Chen, Z.; Yang, X. B.; Yang, Z. Q. High-Speed Efficient Terahertz Modulation Based on Tunable Collective-Individual State Conversion within an

- Active 3 nm Two-Dimensional Electron Gas Metasurface. *Nano Lett.* **2019**, *19*, 7588–7597.
- (34) Hu, Y.; Tong, M.; Hu, S.; He, W.; Cheng, X. A.; Jiang, T. Multidimensional engineered metasurface for ultrafast terahertz switching at frequency-agile channels. *Nanophotonics* **2022**, *11*, 1367–1378.
- (35) Shen, N.; Massaouti, M.; Gokkavas, M.; Manceau, J.; Ozbay, E.; Kafesaki, M.; Koschny, T.; Tzortzakos, S.; Soukoulis, C. M. Optically Implemented Broadband Blueshift Switch in the Terahertz Regime. *Phys. Rev. Lett.* **2011**, *106*, 037403.
- (36) Tang, K.; Su, Y.; Qin, M.; Zhai, X.; Wang, L. Dynamically tunable coherent perfect absorption and transparency in Dirac semimetal metasurface. *Opt. Mater. Express* **2019**, *9*, 3649–3656.
- (37) Nouman, M. T.; Kim, H.; Woo, J. M.; Hwang, J. H.; Kim, D.; Jang, J. Terahertz Modulator based on Metamaterials integrated with Metal-Semiconductor-Metal Varactors. *Sci. Rep.* **2016**, *6*, 26452.
- (38) Alius, H.; Dodel, G. Amplitude-phase-and frequency modulation of far-infrared radiation by optical excitation of silicon. *Infrared Phys.* **1991**, *32*, 1–11.
- (39) Pitchappa, P.; Kumar, A.; Prakash, S.; Jani, H.; Venkatesan, T.; Singh, R. Chalcogenide Phase Change Material for Active Terahertz Photonics. *Adv. Mater.* **2019**, *31*, 1808151.1–7.
- (40) Wang, Q.; Rogers, E. T. F.; Gholipour, B.; Wang, C.; Yuan, G.; Teng, J.; Zheludev, N. I. Optically reconfigurable metasurfaces and photonic devices based on phase change materials. *Nat. Photonics* **2016**, *10*, 60–65.
- (41) Okada, T.; Tanaka, K. Photo-designed terahertz devices. *Sci. Rep.* **2011**, *1*, 121.
- (42) Xie, Z.; Wang, X.; Ye, J.; Feng, S.; Sun, W.; Akalin, T.; Zhang, Y. Spatial Terahertz Modulator. *Sci. Rep.* **2013**, *3*, 3347.
- (43) Jing, X.; Gui, X.; Zhou, P.; Hong, Z. Physical Explanation of Fabry-Pérot Cavity for Broadband Bilayer Metamaterials Polarization Converter. *J. Lightwave Technol.* **2018**, *36*, 2322–2327.
- (44) Liu, W.; Chen, S.; Li, Z.; Cheng, H.; Yu, P.; Li, J.; Tian, J. Realization of broadband cross-polarization conversion in transmission mode in the terahertz region using a single-layer metasurface. *Opt. Lett.* **2015**, *40*, 3185–3188.
- (45) Xia, R.; Jing, X.; Gui, X.; Tian, Y.; Hong, Z. Broadband terahertz half-wave plate based on anisotropic polarization conversion metamaterials. *Opt. Mater. Express* **2017**, *7*, 977.
- (46) Wen, X.; Zheng, J. Broadband THz reflective polarization rotator by multiple plasmon resonances. *Opt. Express* **2014**, *22*, 28292–28300.
- (47) Li, J.; Zheng, C.; Li, J.; Wang, G.; Liu, J.; Yue, Z.; Hao, X.; Yang, Y.; Li, F.; Tang, T.; Zhang, Y.; Zhang, Y.; Yao, J. Terahertz wavefront shaping with multi-channel polarization conversion based on all-dielectric metasurface. *Photonics Res.* **2021**, *9*, 1939–1947.
- (48) Luo, X. Q.; Hu, F. R.; Li, G. Y. Broadband switchable terahertz half-/quarter-wave plate based on VO₂-metal hybrid metasurface with over/underdamped transition. *J. Phys. D Appl. Phys.* **2021**, *54*, 505111.
- (49) Ding, F.; Zhong, S.; Bozhevolnyi, S. I. Vanadium Dioxide Integrated Metasurfaces with Switchable Functionalities at Terahertz Frequencies. *Adv. Opt. Mater.* **2018**, *6*, 1701204.
- (50) Wang, Y.; Li, S.; Wang, H.; Feng, L.; Tan, B.; Tan, Y.; Su, R.; Wu, J.; Zhang, C.; Jin, B.; Chen, J.; Wu, P. Broadband and efficient asymmetric wavefront manipulation via terahertz polarization-selective metasurface. *Appl. Phys. Lett.* **2022**, *121*, 151701.
- (51) Ameling, R.; Giessen, H. Microcavity plasmonics: strong coupling of photonic cavities and plasmons. *Laser Photon. Rev.* **2013**, *7*, 141–169.
- (52) Chen, H.; Wang, J.; Ma, H.; Qu, S.; Xu, Z.; Zhang, A.; Yan, M.; Li, Y. Ultra-wideband polarization conversion metasurfaces based on multiple plasmon resonances. *J. Appl. Phys.* **2014**, *115*, 154504.
- (53) Gao, X.; Han, X.; Cao, W. P.; Li, H. O.; Ma, H. F.; Cui, T. J. Ultrawideband and High-Efficiency Linear Polarization Converter Based on Double V-Shaped Metasurface. *IEEE T. Antenn. Propag.* **2015**, *63*, 3522–3530.
- (54) Chen, H.; Taylor, A. J.; Yu, N. A review of metasurfaces: physics and applications. *Rep. Prog. Phys.* **2016**, *79*, 076401.
- (55) Smith, D. R.; Vier, D. C.; Koschny, T.; Soukoulis, C. M. Electromagnetic parameter retrieval from inhomogeneous metamaterials. *Phys. Rev. E* **2005**, *71*, 36617.
- (56) Schroeder, W.; Wolff, I. The origin of spurious modes in numerical solutions of electromagnetic field eigenvalue problems. *IEEE T. Microw. Theory* **1994**, *42*, 644–653.
- (57) Cui, T. J.; Qi, M. Q.; Wan, X.; Zhao, J.; Cheng, Q. Coding metamaterials, digital metamaterials and programmable metamaterials. *Light-Sci & Appl.* **2014**, *3*, No. e218.
- (58) Chen, H. T. Interference theory of metamaterial perfect absorbers. *Opt. Express* **2012**, *20*, 7165–7271.
- (59) Liu, E.; Zhu, B.; Luo, J. *The Physics of Semiconductors*; Publishing House of Electronics Industry: Beijing, 2011; pp 1–16.
- (60) Staude, I.; Schilling, J. Metamaterial-inspired silicon nanophotonics. *Photonics* **2017**, *11*, 274–284.
- (61) Reed, G. T.; Mashanovich, G.; Gardes, F. Y.; Thomson, D. J. Erratum: Silicon optical modulators. *Nat. Photonics* **2010**, *4*, 660.
- (62) Heyes, J. E.; Withayachumnankul, W.; Grady, N. K.; Chowdhury, D. R.; Azad, A. K.; Chen, H. T. Hybrid metasurface for ultra-broadband terahertz modulation. *Appl. Phys. Lett.* **2014**, *105*, 181108.
- (63) Chen, H.; O'Hara, J. F.; Azad, A. K.; Taylor, A. J.; Averitt, R. D.; Shrekenhamer, D. B.; Padilla, W. J. Experimental demonstration of frequency-agile terahertz metamaterials. *Nat. Photonics* **2008**, *2*, 295–298.
- (64) Lou, J.; Xu, X.; Huang, Y.; Yu, Y.; Wang, J.; Fang, G.; Liang, J.; Fan, C.; Chang, C. Optically Controlled Ultrafast Terahertz Metadevices with Ultralow Pump Threshold. *Small* **2021**, *17*, 2104275.
- (65) Tong, Y.; Wang, S.; Song, X.; Yang, L.; Yao, J.; Ye, Y.; Ren, Y.; Zhang, Y.; Xin, S.; Ren, X. Multi-band tunable terahertz absorber based on metamaterial. *J. Infrared Millim. W.* **2020**, *39*, 735–741.
- (66) Shen, X.; Cui, T. J. Photoexcited broadband redshift switch and strength modulation of terahertz metamaterial absorber. *J. Optics* **2012**, *14*, 114012.
- (67) Siday, T.; Vabishchevich, P. P.; Hale, L.; Harris, C. T.; Luk, T. S.; Reno, J. L.; Brener, I.; Mitrofanov, O. Terahertz Detection with Perfectly-Absorbing Photoconductive Metasurface. *Nano Lett.* **2019**, *19*, 2888–2896.
- (68) Fan, K.; Padilla, W. J. Dynamic electromagnetic metamaterials. *Mater. Today* **2015**, *18*, 39–50.
- (69) Hashemi, M. R.; Cakmakyan, S.; Jarrahi, M. Reconfigurable metamaterials for terahertz wave manipulation. *Rep. Prog. Phys.* **2017**, *80*, 094501.
- (70) Hu, Y. Z.; Jiang, T.; Sun, H.; Tong, M. Y.; You, J.; Zheng, X.; Xu, Z. J.; Cheng, X. A. Terahertz Metaphotonic Devices: Ultrafast Frequency Shift of Electromagnetically Induced Transparency in Terahertz Metaphotonic Devices. *Laser Photon. Rev.* **2020**, *14*, 2100244.
- (71) Cai, H.; Huang, Q.; Hu, X.; Liu, Y.; Fu, Z.; Zhao, Y.; He, H.; Lu, Y. All-Optical and Ultrafast Tuning of Terahertz Plasmonic Metasurfaces. *Adv. Opt. Mater.* **2018**, *6*, 1800143.
- (72) Doany, F. E.; Grischkowsky, D.; Chi, C. C. Carrier lifetime versus ion-implantation dose in silicon on sapphire. *Appl. Phys. Lett.* **1987**, *50*, 460–462.
- (73) Cho, K.; Numan, M.; Finstad, T. G.; Chu, W. K.; Liu, J.; Wortman, J. J. Transient enhanced diffusion during rapid thermal annealing of boron implanted silicon. *Appl. Phys. Lett.* **1985**, *47*, 1321–1323.
- (74) Chen, Z. C.; Hong, M. H.; Lim, C. S.; Han, N. R.; Shi, L. P.; Chong, T. C. Parallel laser microfabrication of large-area asymmetric split ring resonator metamaterials and its structural tuning for terahertz resonance. *Appl. Phys. Lett.* **2010**, *96*, 181101.
- (75) Uhd Jepsen, P.; Schairer, W.; Libon, I. H.; Lemmer, U.; Hecker, N. E.; Birkholz, M.; Lips, K.; Schall, M. Ultrafast carrier trapping in microcrystalline silicon observed in optical pump-terahertz probe measurements. *Appl. Phys. Lett.* **2001**, *79*, 1291–1293.

(76) Liu, X.; Liu, H.; Sun, Q.; Huang, N. Metamaterial terahertz switch based on split-ring resonator embedded with photoconductive silicon. *Appl. Opt.* **2015**, *54*, 3478–3483.

(77) Sjodin, T.; Petek, H.; Dai, H. L. Ultrafast Carrier Dynamics in Silicon: A Two-Color Transient Reflection Grating Study on a (111) Surface. *Phys. Rev. Lett.* **1998**, *81*, 5664–5667.

(78) Myers, K. E.; Wang, Q.; Dexheimer, S. L. Ultrafast carrier dynamics in nanocrystalline silicon. *Phys. Rev. B: Condens. Matter Mater. Phys.* **2001**, *64*, 161309.